Nuclear Engineering and Technology xxx (xxxx) xxx

Contents lists available at ScienceDirect

Nuclear Engineering and Technology

journal homepage: www.elsevier.com/locate/net

Original Article

Comparison of $LaBr_3$:Ce and $CeBr_3$ scintillators for ^{55}Fe detection

Jae Hyung Park [a], Siwon Song [a], Seunghyeon Kim [a], Sangjun Lee [a], Jinhong Kim [a], Cheol Ho Pyeon [b], Sin Kim [a], Bongsoo Lee [a,*]

[a] School of Energy Systems Engineering, Chung-Ang University, 06974, Seoul, South Korea
[b] Research Center for Safe Nuclear System, Institute for Integrated Radiation and Nuclear Science, Kyoto University, Asashiro-nishi, Kumatori-cho, Sennan-gun, 590-0494, Osaka, Japan

ARTICLE INFO

Keywords:
$LaBr_3$:Ce
$CeBr_3$
^{55}Fe
Low-energy X-ray
Gamma-ray spectroscopy

ABSTRACT

The detection capability for ^{55}Fe was compared using 1" × 1″ $LaBr_3$:Ce and $CeBr_3$ scintillators. To enable low-energy X-ray measurements, the top of the scintillator housing was modified with a beryllium window, allowing the detection of a 5.9 keV peak, verified through comparison with the intrinsic background spectrum. This peak was also observed in simultaneous measurements with ^{137}Cs and ^{60}Co. Detection capabilities were further evaluated using the significance method and minimum detectable activity analysis. Consequently, $LaBr_3$:Ce exhibited faster detection of the 5.9 keV peak and higher detection efficiency compared to $CeBr_3$. Even when the influence of ^{138}La decay was excluded, $LaBr_3$:Ce outperformed $CeBr_3$ under multi-source conditions. However, its intrinsic background resulted in a higher minimum detectable activity, rendering it less sensitive than $CeBr_3$ for radioactivity measurement.

1. Introduction

With the active decommissioning and decontamination (D&D) of aging nuclear power plants worldwide, attention is increasingly focused on the radioactive aerosols generated during these processes. Primary sources of radioactive aerosols in D&D include cutting and melting radioactive metal structures and wastes [1]. Radionuclides such as ^{3}H, ^{55}Fe, ^{60}Co, and ^{63}Ni, which pose risks to workers, vary depending on factors such as the type and composition of the metal, the cutting methods employed, and the overall decommissioning strategy [1,2].

^{55}Fe, which emits 5.9 keV X-rays and has a half-life of 2.7 yr, is primarily produced by neutron activation of stable ^{54}Fe and ^{56}Fe in reactor components. Given the extensive use of iron-containing materials, including concrete, in nuclear power plant construction, ^{55}Fe is among the most prevalent radionuclides in decommissioning wastes [3–5]. Despite its low energy emission, ^{55}Fe is anticipated to be a major contributor to the effective dose coefficient [1,6], necessitating a quantitative assessment to ensure safe and effective decommissioning processes and reliable exposure control for the personnel involved.

The most common method for ^{55}Fe determination is liquid scintillation counting, which offers high counting efficiency for the low-energy X-rays and Auger electrons from ^{55}Fe [7]. However, this approach requires sophisticated radiochemical techniques to separate ^{55}Fe from other nuclides, making it highly time-consuming and potentially requiring additional steps depending on the method and target sample [4,5,7,8]. For instance, to extract the target nuclide from a sample with a high quartz content, sufficient hydrofluoric acid must be used, which makes the chemical separation and purification process very challenging. In the case of alkali fusion method, the alkali compounds used to degrade the sample necessitate an additional process to remove alkali metals from the solution. Recently, accelerator mass spectrometry has been employed to detect ^{55}Fe without pretreatment, but this method is costly and slow resulting in low throughput [4]. These methods are laboratory-based and are not suitable for workplace applications due to the complexity of the process and configuration.

Scintillation detectors are among the most widely utilized tools for in-situ radiation measurements [9]. Among these, the scintillators $LaBr_3$:Ce and $CeBr_3$ are widely regarded as optimal choices for gamma-ray detection across various fields, particularly in gamma-ray spectroscopy, owing to their short decay times, high light yields, and excellent energy resolution [10,11]. Additionally, they are commonly used as detection units in radiological surveying, environmental monitoring, and unmanned survey systems because of their operational stability and compatibility with diverse platforms [12–15].

$LaBr_3$:Ce and $CeBr_3$ exhibit similar performance in most aspects but are frequently compared due to the presence or absence of intrinsic

* Corresponding author.
E-mail address: bslee@cau.ac.kr (B. Lee).

https://doi.org/10.1016/j.net.2025.103506
Received 24 November 2024; Received in revised form 13 January 2025; Accepted 23 January 2025
Available online 24 January 2025

radioactivity from ^{138}La. This distinction is particularly significant in gamma-ray spectroscopy conducted within the energy range below 1.6 MeV. Quarati et al. compared the figure of merit of $LaBr_3$:Ce and $CeBr_3$ across the energy range of 20 keV to 3 MeV and concluded that, on average, $LaBr_3$:Ce requires four to five times longer measurement times to achieve comparable confidence levels [11]. Additionally, Milbrath et al. reported that the 1436 keV gamma-rays from ^{138}La negatively affect the sensitivity of $LaBr_3$:Ce for the detection of ^{40}K [16]. However, most studies, including those mentioned, have focused on the application of radio-isotope identification devices and radiation monitor for hazardous material control and emergency response, limiting the target nuclides to isotopes such as ^{131}I, ^{134}Cs, ^{137}Cs, without considering ^{55}Fe [13,16–19]. Notably, ^{138}La emits not only 1436 keV gamma-rays but also 5.6 keV and 37.4 keV X-rays, necessitating an evaluation of its impact when comparing the detection capability for the 5.9 keV X-rays emitted by ^{55}Fe [20]. In studies developing gamma-ray detectors for satellite applications, $LaBr_3$:Ce has been used to measure the energy spectrum of ^{55}Fe; however, these studies did not specifically account for the influence of ^{138}La [21–24].

In this study, we compared the detection capabilities of $LaBr_3$:Ce and $CeBr_3$ for ^{55}Fe through energy spectral measurements. To facilitate low-energy X-ray detection, part of the scintillator housing was modified with a beryllium window, while the rest of the setup was consistent with a conventional scintillation spectrometer. Detection of ^{55}Fe was verified by comparison with the intrinsic background, and significance testing and minimum detectable activity (MDA) analysis were conducted for the identified peaks to evaluate the low-energy X-ray detection performance of the two scintillators.

2. Materials and methods

In this study, 1" × 1″ cylindrical $LaBr_3$:Ce and $CeBr_3$ scintillators, manufactured by Epic Crystal, were utilized. Each scintillator was encapsulated within an aluminum housing featuring a 200 μm-thick beryllium window at the top. The beryllium window, due to its low mass absorption coefficient, provides better X-ray transmission compared to the aluminum of the housing, enabling the detection of weakly penetrating radiation [25,26]. A Hamamatsu H10828 photomultiplier tube (PMT) served as the light detection device, with an optical pad (EJ-560, Eljen Technology) applied at the interface between the scintillator and the PMT window to ensure optimal light transmission. A polyacetal shading case was fabricated to block external light and secure the scintillator-PMT assembly, with a hole incorporated in the section adjacent to the beryllium window to prevent interference with low-energy radiation transmission. The detailed configuration of the detector assembly and the properties of the scintillators are presented in Fig. 1 and Table 1, respectively.

The output signal from the PMT was amplified using a charge-sensitive preamplifier (CR-113, Cremat Inc.) and recorded by a digitizer (DT5725, CAEN). Data acquisition was conducted via MC^{2}Analyzer software, with a trapezoidal rise time of 3 μs, corresponding to the shaping time of the analog acquisition chain [28]. The PMT bias voltage was set to −740 V for $LaBr_3$:Ce and −790 V for $CeBr_3$, with all measurements taken over a 1200-s duration. The radiation sources used in this study were all manufactured by Spectrum Techniques. The ^{55}Fe source was a laminate disk source with dimensions of 25.4 × 0.51 mm, while the ^{137}Cs and ^{60}Co sources were standard disk sources with dimensions of 25.4 × 3.2 mm. The experiment was conducted in a dark-room where external light was blocked, and no additional measures were taken for external radiation shielding or radiation collimation.

3. Experimental results

The spectra measured for the intrinsic backgrounds of $LaBr_3$:Ce and $CeBr_3$, and for the ^{55}Fe radioactive source, are shown in Fig. 2. The ^{55}Fe source, with an activity of 4.077 μCi, was positioned 5 mm from the

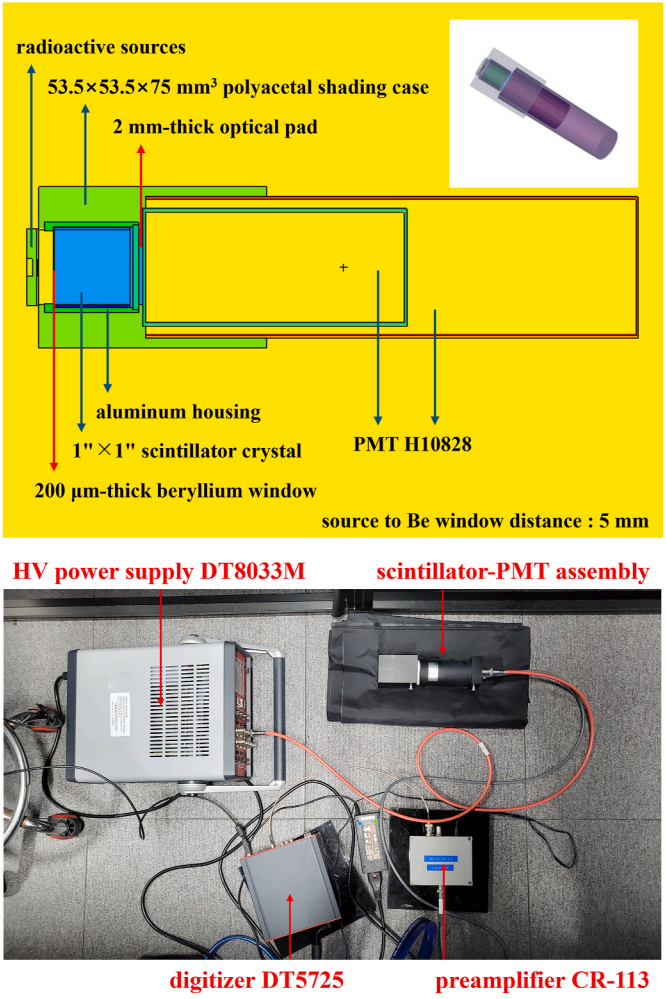

Fig. 1. Configuration of the scintillator-PMT assembly and the experimental setup.

Table 1
Physical properties of $LaBr_3$:Ce and $CeBr_3$ [27].

Property	$LaBr_3$:Ce	$CeBr_3$	Unit
Density	5.2	5.1	g/cm^3
Melting point	1116	1056	K
Emission peak	380	380	nm
Light output	68,000	60,000	ph/MeV
Decay constant	16	20	ns
Hygroscopic	yes	yes	–
Refractive index	1.9	2.1	–

beryllium window of the scintillator, aligned with a hole in the shading case. Both sets of results clearly distinguish the spectra with and without the ^{55}Fe source especially in comparison with the 5.6 keV peak from the decay of ^{138}La in the $LaBr_3$:Ce background spectrum [20]. This indicates that the difference is due to the 5.9 keV X-rays emitted by ^{55}Fe.

Fig. 3 shows the variation of the 5.9 keV peak across varying PMT bias voltages. For both $LaBr_3$:Ce and $CeBr_3$, the peak centroid channel increases consistently with higher voltages. Initially, the peak centroid count increases with voltage but eventually decreases, suggesting that the 5.9 keV peak was obscured by system threshold and instrumental noise, including dark current, at lower voltages. At higher voltages, the peak becomes more distinct, highlighting the importance of optimal voltage control in low-energy measurements. However, for $CeBr_3$, additional voltage increases resulted in amplified noise and peak

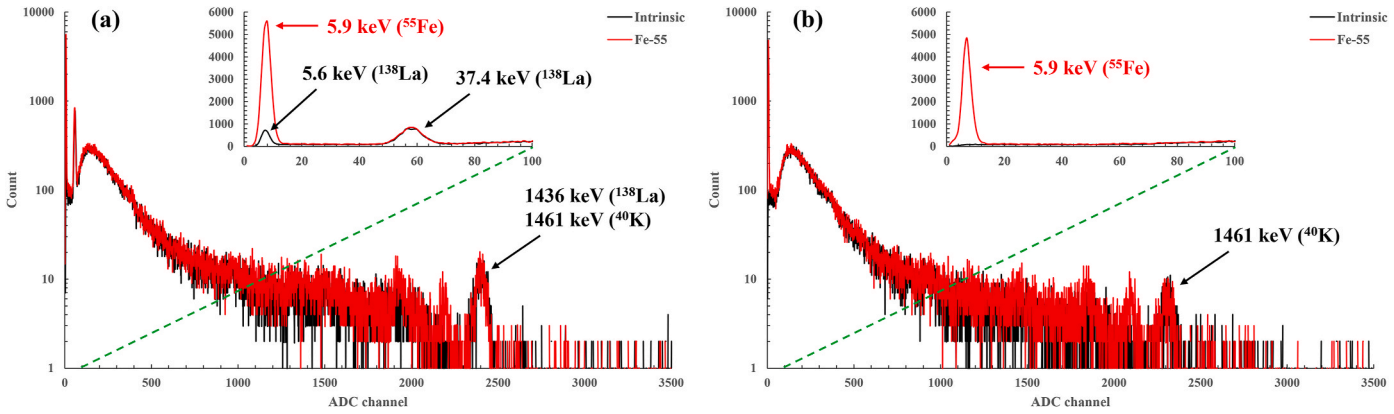

Fig. 2. Pulse height spectra of intrinsic background and ^{55}Fe collected with (a) $LaBr_3$:Ce and (b) $CeBr_3$.

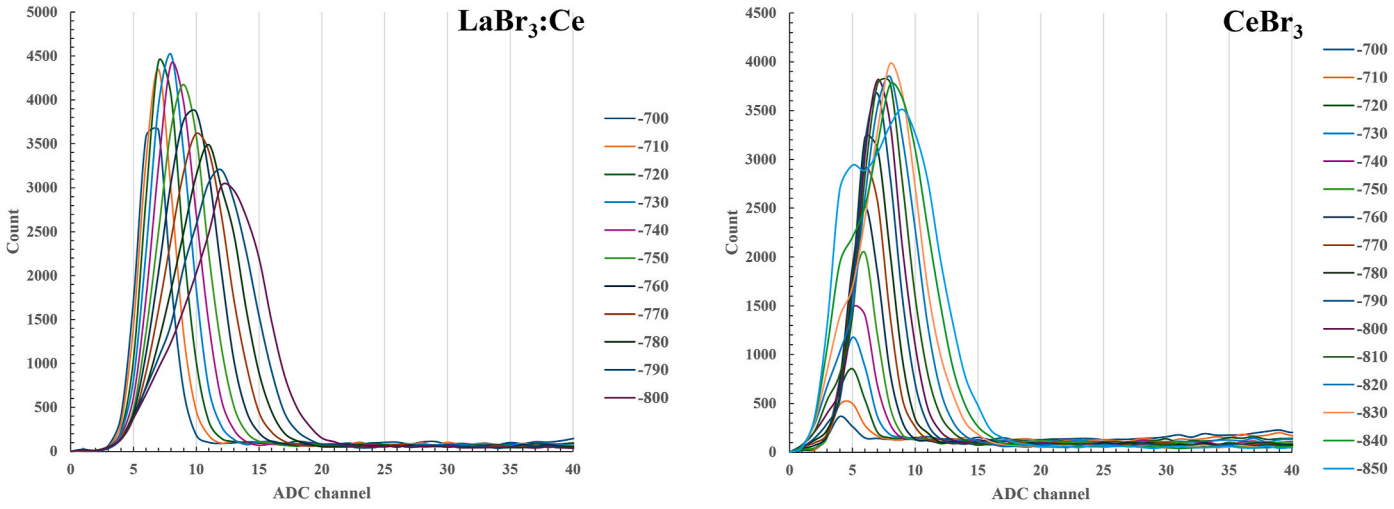

Fig. 3. Variation of the 5.9 keV peak regarding the PMT bias voltage.

distortion, indicating that optimal voltages differ between scintillators. For energy calibration, we used four primary photopeaks (32, 661.657, 1173.228, and 1332.492 keV) derived from ^{137}Cs and ^{60}Co measurements. The radioactivity of the ^{137}Cs and ^{60}Co sources was 0.238 μCi and 0.757 μCi, respectively, and the corresponding calibration spectra are shown in Fig. 4.

^{137}Cs, ^{60}Co, along with ^{55}Fe, are prevalent in decommissioning waste and aerosol samples from nuclear plant dismantling [1,3–5]. Although these radionuclides emit gamma-rays with much higher energies than ^{55}Fe, they are commonly found in decommissioning waste. This implies a high likelihood of their simultaneous detection as background radiation at sites where ^{55}Fe measurement is required. Furthermore, the gamma-rays from these nuclides create a broad continuum extending into the low-energy region, necessitating an evaluation of the impact on the 5.9 keV peak when measured alongside these major radionuclides. Simultaneous measurements of ^{137}Cs, ^{60}Co, and ^{55}Fe are presented in Fig. 5, with the inset highlighting the low-energy region of the spectrum, where the 5.9 keV peak from ^{55}Fe is visible. The inset shows the 0–60 keV region, where the 5.9 keV peak of ^{55}Fe, the 32 keV peak of ^{137}Cs, the 37.4 keV peak of ^{138}La, as well as the continuum and scattering peaks

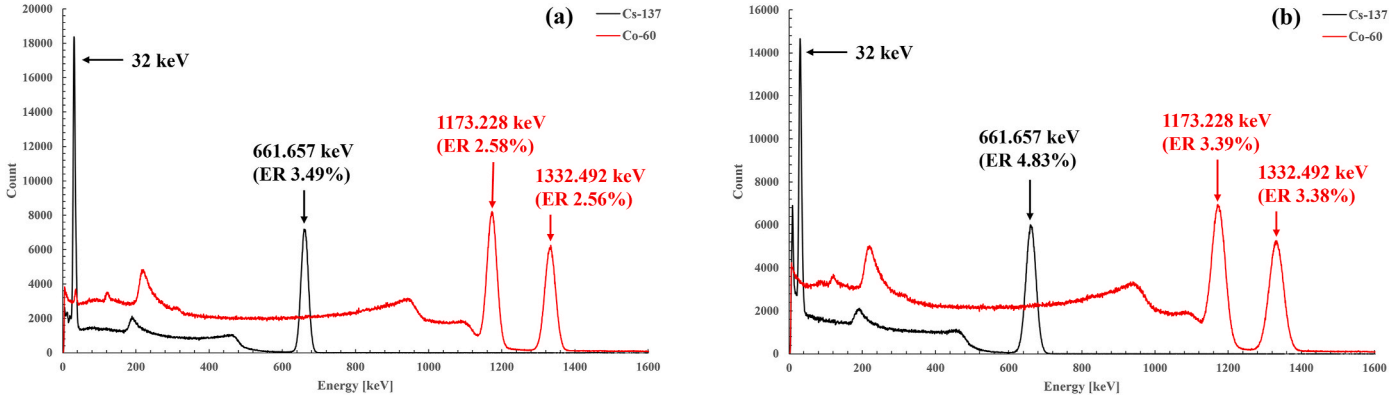

Fig. 4. Energy spectra of ^{137}Cs and ^{60}Co measured with a) $LaBr_3$:Ce and b) $CeBr_3$.

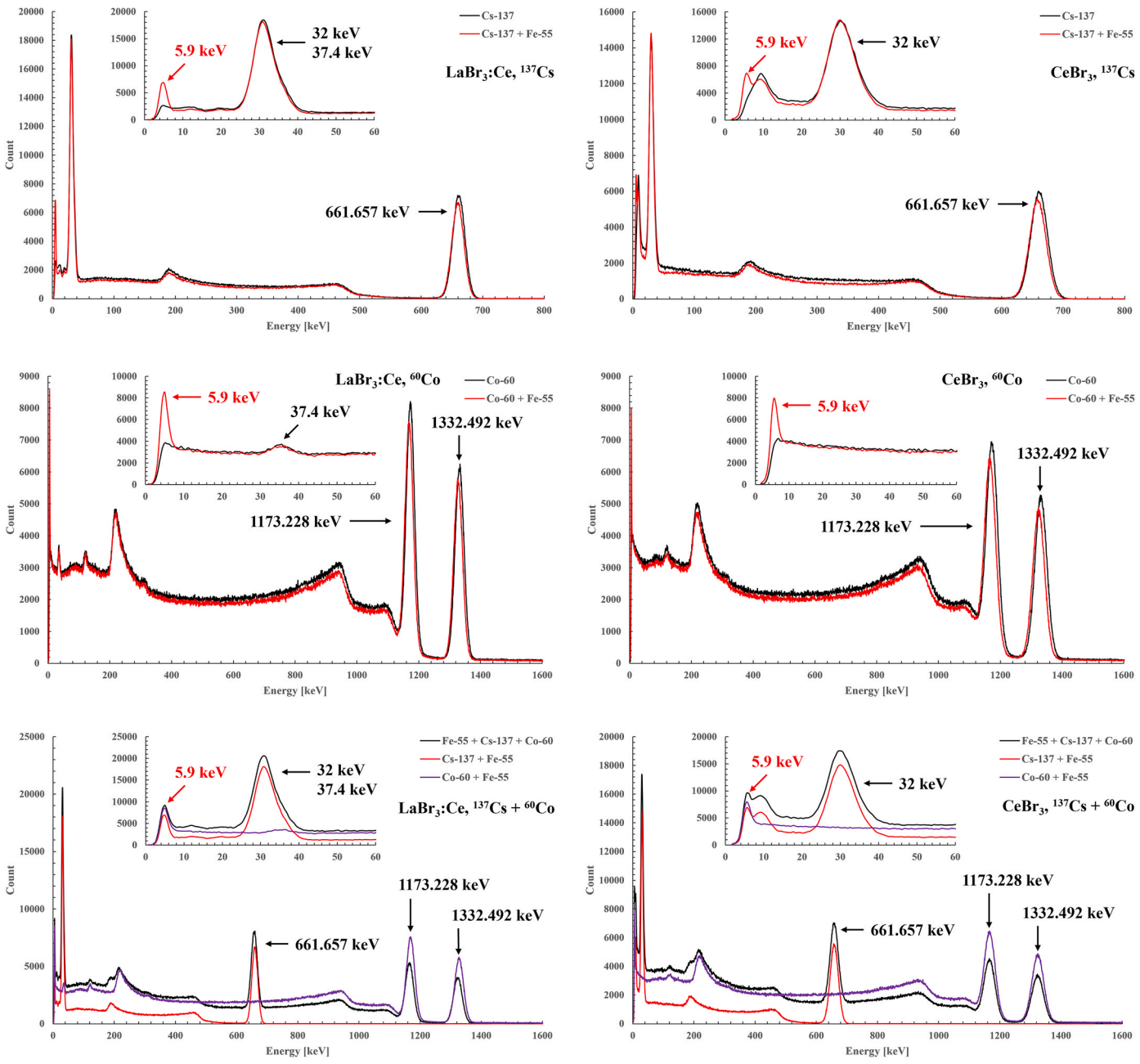

Fig. 5. Energy spectra of simultaneous measurements with $LaBr_3$:Ce and $CeBr_3$.

caused by other gamma and X-rays, can be observed. As observed in background spectra, clear distinctions appear between measurements with and without the ^{55}Fe source. The primary photopeaks, including the low-energy 5.9 keV peak, are evident across all measurement scenarios, confirming that both $LaBr_3$:Ce and $CeBr_3$ scintillators effectively support simultaneous detection of low-energy radiation, even in the presence of high-energy sources.

To assess the ^{55}Fe detection capabilities of the $LaBr_3$:Ce and $CeBr_3$ scintillators, we used the significance method introduced by Milbrath et al. [16]. This method calculates the significance value (Sig_{quan}) for the 5.9 keV peaks observed in the ^{55}Fe measurements, individually and in simultaneous measurements with ^{137}Cs and ^{60}Co. The significance value, representing the extent to which a peak deviates from the background uncertainty, is defined as

$$Sig_{quan} = net\ counts \Big/ net\ error, \tag{1}$$

$$net\ error \approx \sqrt{background + gross\ area}, \tag{2}$$

where the gross area is the total counts in the peak, comprising both net counts and background.

Significance represents the observability of a peak by comparing its net intensity with its uncertainty. It is utilized to confirm the statistical meaning of a peak through simple count summation, calculate the centroid, and validate its recognition as a peak in spectroscopic software, or to compare the performance of different software systems [16,29,30]. The net count and background count used in Equations (1) and (2) are measured simultaneously, meaning that significance is finally proportional to the square root of the measurement time. In other words, if one detector measures a significance value twice as large as another detector within the same measurement time, it implies that the first detector requires only one-fourth of the time to achieve the same significance as the second detector. Furthermore, as the resolution of a

detector improves, the background within the gross peak decreases, resulting in improved significance. These factors make significance a valuable metric for comparing the overall performance of detectors.

Table 2 compares the ^{55}Fe measurement results for both scintillators under identical conditions over a 1200-s duration. $LaBr_3$:Ce consistently demonstrated better performance, suggesting that achieving a comparable 5.9 keV peak significance using $CeBr_3$ would require approximately 1.3–1.5 times longer measurement duration. However, these results include the 5.6 keV peak from the intrinsic background of $LaBr_3$:Ce, arising from ^{138}La decay, which may have led to an overestimated significance for this scintillator. To address this, we recalculated the significance by subtracting the intrinsic background spectra of each scintillator and the spectra from ^{137}Cs and ^{60}Co measurements alone from the ^{55}Fe and simultaneous measurement spectra. The adjusted significance is defined as follows:

$$Sig = net\ counts / \sqrt{gross\ area}\ . \tag{3}$$

The adjusted significance indicates that when the background is well known and removed from the spectrum, the net uncertainty of the peak depends solely on the gross area of the peak rather than the sum of gross area and the background. Table 3 presents the recalculated significance values following background subtraction, which reveals a notable decrease in the significance for $LaBr_3$:Ce compared to the initial results. With this correction, $CeBr_3$ shows an improvement in significance for ^{137}Cs measurements, narrowing the performance gap between the two scintillators. Nonetheless, $LaBr_3$:Ce maintains a slight advantage in concurrent measurement scenarios, underscoring its suitability for ^{55}Fe detection in multi-source environments, provided the intrinsic background is sufficiently pre-measured. Radiation sources in decommissioning sites often coexist as multiple types rather than a single source, and due to its better simultaneous measurement results with the two most likely radionuclides, $LaBr_3$:Ce can be considered more effective for field applications.

To further evaluate the radioactivity detection capabilities of each scintillator, we calculated the MDA based on the data in Table 3. The MDA, defined as the minimum level of activity that a system can reliably detect in specific conditions, is a key parameter in assessing the capabilities of gamma-ray spectrometers for radioactivity measurements. Detection efficiency was derived from these results, and MDA was calculated using the Currie method [31]. Owing to the distinct background characteristics of $LaBr_3$:Ce (peaked) and $CeBr_3$ (non-peaked), the MDA for each scintillator was computed using the following equations:

$$MDA_{peaked} = \frac{2.71 + 3.29\sqrt{B + B \bullet \frac{N}{2m}}}{\varepsilon \bullet p \bullet t}, \tag{4}$$

$$MDA_{non-peaked} = \frac{2.71 + 3.29\sqrt{2 \bullet B}}{\varepsilon \bullet p \bullet t}, \tag{5}$$

where B represents the background count, ε is the detection efficiency, p is the emission probability, t is the measurement live time, N denotes the number of channels in the region of interest, and m represents the number of channels used for background estimation [32,33].

Table 4 presents the detection efficiency and MDA for the 5.9 keV peak of ^{55}Fe, highlighting that $LaBr_3$:Ce has a higher efficiency than $CeBr_3$, even when excluding contributions from the ^{138}La background. Despite the proximity and high radioactivity of the ^{55}Fe source, the low overall detection efficiency is likely due to the short attenuation length of low-energy X-rays, surface effects on the scintillator, and information loss within the crystal bulk [34,35]. Although both scintillators show somewhat high MDA values due to low detection efficiency, $LaBr_3$:Ce has a higher MDA value owing to its intrinsic background. This suggests that $LaBr_3$:Ce may be less sensitive to radioactivity measurement than $CeBr_3$. However, since MDA decreases with longer measurement times, this difference is expected to narrow, such as a few becquerels, making $LaBr_3$:Ce a viable option for long-term applications such as monitoring, where measurement duration can be extended to achieve lower detection thresholds.

4. Conclusion

This study evaluates the detection capabilities of $LaBr_3$:Ce and $CeBr_3$ scintillators with beryllium windows for low-energy X-rays from ^{55}Fe. Compared with the intrinsic background spectrum, energy spectra analysis confirmed the presence of a 5.9 keV peak, which was clearly identified in simultaneous measurements with other radioactive sources. By applying the significance method and MDA analysis, we found that $LaBr_3$:Ce had faster detection and higher efficiency for ^{55}Fe than $CeBr_3$, despite its intrinsic radioactivity from ^{138}La decay. However, $LaBr_3$:Ce showed a higher MDA than $CeBr_3$, indicating a slightly reduced sensitivity for radioactivity measurement. This difference is still expected to be negligible in long-term measurement applications.

$LaBr_3$:Ce and $CeBr_3$ exhibit similar overall performance, with only minor differences, as reflected in the slight variations observed in the significance results of this study. However, detection sensitivity differences arise due to intrinsic background, with $LaBr_3$:Ce typically considered inferior due to the presence of ^{138}La. Contrary to expectations, $LaBr_3$:Ce demonstrated better results for detecting 5.9 keV X-rays, regardless of background influence, prompting a reconsideration of its potential. The intrinsic background of the scintillator can be more precisely determined through extended measurement times, and $LaBr_3$:Ce offers the best energy resolution among commercially available scintillators. It also outperformed $CeBr_3$ in simultaneous measurements with other radionuclides, providing a clearer 5.9 keV peak, and is slightly more cost-effective. Although further evaluation with dominant radionuclides, depending on decommissioning strategies, may be necessary, $LaBr_3$:Ce is deemed more suitable for field-deployable systems capable of detecting ^{55}Fe.

The scintillator dimensions used in this study reflect typical spectrometer sizes, confirming that standard scintillation spectrometers can effectively detect low-energy sources like ^{55}Fe. This capability suggests the potential for broader applications of scintillation spectrometers. For instance, scintillation spectrometers can be used to analyze filters that capture radioactive aerosols generated at decommissioning sites, providing real-time information on low-energy emitters such as ^{55}Fe directly at the work site to ensure worker safety. Moreover, in synergy

Table 2
Significance comparison of $LaBr_3$:Ce and $CeBr_3$ for ^{55}Fe measurements.

Factor	$LaBr_3$:Ce			$CeBr_3$		
	^{55}Fe	^{55}Fe,^{137}Cs	^{55}Fe,^{60}Co	^{55}Fe	^{55}Fe,^{137}Cs	^{55}Fe,^{60}Co
FWHM	2.37	2.38	2.55	2.63	1.51	2.57
Gross area	23224	34940	48143	19610	28671	45989
Net area	22448	25387	30027	18385	9236	24527
Background	776	9553	18116	1225	19435	21462
Error	154.92	210.93	257.41	144.34	219.33	259.71
Sig_{quan}	144.90	120.36	116.65	127.37	42.11	94.44

*FWHM, full width at half maximum.

Table 3
Significance comparison after comparable background subtraction.

Factor	$LaBr_3$:Ce			$CeBr_3$		
	^{55}Fe	^{55}Fe,^{137}Cs	^{55}Fe,^{60}Co	^{55}Fe	^{55}Fe,^{137}Cs	^{55}Fe,^{60}Co
Gross area	23224	34940	48143	19610	28671	45989
Net area	19951	16413	19046	18576	14057	17068
Background	3273	18527	29097	1034	14614	28921
Sig	130.92	87.81	86.80	132.65	83.02	79.59

Table 4
Measurement capabilities of each scintillator for ^{55}Fe.

Factor	$LaBr_3$:Ce	$CeBr_3$
Measurement live time	1200 s	1200 s
Detection efficiency	4.04E-04 ± 8.18E-05	3.77E-04 ± 7.62E-05
MDA	1557 Bq	1134 Bq

†MDA, minimum detectable activity.

with stability, scintillation spectrometers can facilitate low-energy radiation measurement in diverse environments where the field operation of specialized instruments is challenging. Future studies will assess the detection capability for radioactive material trapped in actual aerosol filters, with a focus on how detection efficiency for low-energy X-rays varies depending on co-existing radiation sources and the dimensions of the scintillator.

CRediT authorship contribution statement

Jae Hyung Park: Writing – original draft, Visualization, Validation, Methodology, Formal analysis, Conceptualization. **Siwon Song:** Software, Investigation, Formal analysis, Data curation. **Seunghyeon Kim:** Software, Investigation, Formal analysis, Data curation. **Sangjun Lee:** Software, Resources, Investigation. **Jinhong Kim:** Software, Resources, Investigation. **Cheol Ho Pyeon:** Writing – review & editing, Validation. **Sin Kim:** Writing – review & editing, Validation. **Bongsoo Lee:** Writing – review & editing, Validation, Supervision, Project administration, Funding acquisition, Conceptualization.

Declaration of interests

The authors declare no conflict of interest.

Acknowledgments

This research was supported by the Basic Science Research Program through the National Research Foundation of Korea (NRF) funded by the Ministry of Education (No. RS-2024-00414355), and the National Research Foundation of Korea (NRF) grant funded by the Korean government (MSIT) (No. 2020M2D2A2062457, 2022M2D4A1084440).

References

[1] Nakkyu Chae, Min-Ho Lee, Sungyeol Choi, Byung Gi Park, Jong-Soon Song, Aerodynamic diameter and radioactivity distributions of radioactive aerosols from activated metals cutting for nuclear power plant decommissioning, J. Hazard Mater. 369 (2019) 727–745, https://doi.org/10.1016/j.jhazmat.2019.02.093.

[2] IAEA, Radiological characterization of shut down nuclear reactors for decommissioning purposes. Technical Reports Series No. 389, International Atomic Energy Agency, 1998.

[3] Xiaolin Hou, Radiochemical analysis of radionuclides difficult to measure for waste characterization in decommissioning of nuclear facilities, J. Radioanal. Nucl. Chem. 273 (2007) 43–48, https://doi.org/10.1007/s10967-007-0708-x.

[4] Silke Merchel, Georg Rugel, Johannes Lachner, Anton Wallner, Diana Walther, René Ziegenrücker, Evaluation of a sensitive, reasonable, and fast detection method for ^{55}Fe in steel, J. Radioanal. Nucl. Chem. 330 (2021) 727–735, https://doi.org/10.1007/s10967-021-08000-7.

[5] Chan-Yeon Lee, Jong-Myoung Lim, Hyuncheol Kim, Da-Young Gam, A study on an optimized pretreatment method for the determination of ^{55}Fe and ^{63}Ni in decommissioning waste samples, J. Radioanal. Nucl. Chem. 332 (2023) 5185–5191, https://doi.org/10.1007/s10967-023-08985-3.

[6] J.C. Evans, E.L. Lepel, R.W. Sanders, C.L. Wilkerson, W. Silker, C.W. Thomas, K. H. Abel, D.R. Robertson, Long-Lived Activation Products in Reactor Materials, NUREG/CR-3474, Pacific Northwest National Laboratory, 1984.

[7] Xiaolin Hou, Lars Frøsig Østergaard, Sven P. Nielsen, Determination of ^{63}Ni and ^{55}Fe in nuclear waste samples using radiochemical separation and liquid scintillating counting, Anal. Chim. Acta 535 (2005) 297–307, https://doi.org/10.1016/j.aca.2004.12.022.

[8] Anumaija Leskinen, Susanna Salminen-Paatero, Antti Räty, Merja Tanhua-Tyrkkö, Taneli Iso-Markku, Esa Puukko, Determination of 14C, 55Fe, 63Ni and gamma emitters in activated RPV steel samples: a comparison between calculations and experimental analysis, J. Radioanal. Nucl. Chem. 323 (2020) 399–413, https://doi.org/10.1007/s10967-019-06937-4.

[9] Khalil Amgarou, Frederic Aspe, Raquel Idoeta, Margarita Herranz, Recommendations for the selection of in situ measurement techniques for radiological characterization in nuclear/radiological installations under decommissioning and dismantling processes, Prog. Nucl. Energy 137 (2021) 103761, https://doi.org/10.1016/j.pnucene.2021.103761.

[10] F. Quarati, A.J.J. Bos, S. Brandenburg, C. Dathy, P. Dorenbos, S. Kraft, R. W. Ostendorf, V. Ouspenski, Alan Owens, X-ray and gamma-ray response of a 2"×2" $LaBr_3$:Ce scintillation detector, Nucl. Instrum. Methods Phys. Res. 574 (2007) 115–120, https://doi.org/10.1016/j.nima.2007.01.161.

[11] F.G.A. Quarati, P. Dorenbos, J. van der Biezen, Alan Owens, M. Selle, L. Parthier, P. Schotanus, Scintillation and detection characteristics of high-sensitivity $CeBr_3$ gamma-ray spectrometers, Nucl. Instrum. Methods Phys. Res. 729 (2013) 596–604, https://doi.org/10.1016/j.nima.2013.08.005.

[12] E. Prieto, R. Casanovas, M. Salvadó, Calibration and performance of a real-time gamma-ray spectrometry water monitor using a $LaBr_3$(Ce) detector, Radiat. Phys. Chem. 144 (2018) 444–450, https://doi.org/10.1016/j.radphyschem.2017.10.008.

[13] Denis Glavič-Cindro, Drago Brodnik, Toni Petrovič, Matjaž Vencelj, Dušan Ponikvar, Steven James Bell, Lynsey Keightley, Selina Woods, Compact radioactive aerosol monitoring device for early warning networks, Appl. Radiat. Isot. 126 (2017) 219–224, https://doi.org/10.1016/j.apradiso.2016.12.036.

[14] Young-Yong Ji, Hee-Yeoul Choi, Wanno Lee, Chang-Jong Kim, Hyun-Sock Chang, Kun-Ho Chung, Application of a $LaBr_3$(Ce) scintillation detector to an environmental radiation monitor, IEEE Trans. Nucl. Sci. 65 (2018) 2021–2028, https://doi.org/10.1109/TNS.2018.2823322.

[15] Yukihisa Sanada, Tadashi Orita, Tatsuo Torii, Temporal variation of dose rate distribution around the Fukushima Daiichi nuclear power station using unmanned helicopter, Appl. Radiat. Isot. 118 (2016) 308–316, https://doi.org/10.1016/j.apradiso.2016.09.008.

[16] B.D. Milbrath, B.J. Choate, J.E. Fast, W.K. Hensley, R.T. Kouzes, J.E. Schweppe, Comparison of $LaBr_3$:Ce and NAI(Tl) scintillators for radio-isotope identification devices, Nucl. Instrum. Methods Phys. Res. 572 (2007) 774–784, https://doi.org/10.1016/j.nima.2006.12.003.

[17] A. Baeza, J.A. Corbacho, J.M. Caballero, M.A. Ontalba, J. Vasco, D. Valencia, Development of an advanced radioactive airborne particle monitoring system for use in early warning networks, J. Radiol. Prot. 37 (2017) 642–658, https://doi.org/10.1088/1361-6498/aa758c.

[18] R. Casanovas, J.J. Morant, M. Salvadó, Development and calibration of a real-time airborne radioactivity monitor using direct gamma-ray spectrometry with two scintillation detectors, Appl. Radiat. Isot. 89 (2014) 102–108, https://doi.org/10.1016/j.apradiso.2014.01.026.

[19] Alfredo de Blas, Juan Toral, Carlos Tapia, Albert Riego, Roger García, Javier Dies, Equipment for the continuous measurement and identification of gamma radioactivity on aerosols, IEEE Trans. Nucl. Sci. 63 (2016) 1526–1530, https://doi.org/10.1109/TNS.2015.2489460.

[20] F.G.A. Quarati, I.V. Khodyuk, C.W.E. van Eijk, P. Quarati, P. Dorenbos, Study of ^{138}La radioactive decays using $LaBr_3$ scintillators, Nucl. Instrum. Methods Phys. Res. 683 (2012) 46–52, https://doi.org/10.1016/j.nima.2012.04.066.

[21] P. Lv, S.L. Xiong, X.L. Sun, J.G. Lv, Y.G. Li, A low-energy sensitive compact gamma-ray detector based on $LaBr_3$ and SiPM for GECAM, J. Instrum. 13 (2018) P08014, https://doi.org/10.1088/1748-0221/13/08/P08014.

[22] Dali Zhang, Xinqiao Li, Shaolin Xiong, Yanguo Li, Xilei Sun, Zhenghua An, Yanbing Xu, Yue Zhu, Wenxi Peng, Huanyu Wang, Fan Zhang, Energy response of GECAM gamma-ray detector based $LaBr_3$:Ce and SiPM array, Nucl. Instrum. Methods Phys. Res. 921 (2019) 8–13, https://doi.org/10.1016/j.nima.2018.12.032.

[23] D.L. Zhang, X.L. Sun, Z.H. An, et al., Dedicated SiPM array for GRD of GECAM, Radiat. Detect. Technol. Methods 6 (2022) 63–69, https://doi.org/10.1007/s41605-021-00299-w.

[24] Y.Q. Liu, K. Gong, X.Q. Li, et al., The data acquisition algorithm designed for the SiPM-based detectors of GECAM satellite, Radiat. Detect. Technol. Methods 6 (2022) 70–77, https://doi.org/10.1007/s41605-021-00311-3.

[25] Brackney Howard, Z.J. Atlee, Beryllium windows for permanently evacuated X-ray tubes, Rev. Sci. Instrum. 14 (1943) 59–63, https://doi.org/10.1063/1.1770125.

[26] G.F. Knoll, Radiation Detection and Measurement, third ed., John Wiley & Sons, Inc., New York, 2000.

[27] Epic Crystal, $LaBr_3$:Ce and $CeBr_3$ scintillators datasheet. Available online: https://www.epic-crystal.com/scintillation-crystals/.

[28] CAEN, MC^2Analyzer User manual. Available online: https://www.caen.it/support-services/documentation-area/?documentbyname=mc2analyzer&type=all-categories.

[29] J.S. Yadav, J. Brückner, J.R. Arnold, Weak peak problem in high resolution gamma-ray spectroscopy, Nucl. Instrum. Methods Phys. Res. 277 (1989) 591–598, https://doi.org/10.1016/0168-9002(89)90793-6.

[30] Cade R. Rodgers, Christian Iliadis, On the analysis of signal peaks in pulse-height spectra, Nucl. Instrum. Methods Phys. Res. 998 (2021) 165172, https://doi.org/10.1016/j.nima.2021.165172.

[31] Lloyd A. Currie, Limits for qualitative detection and quantitative determination. Application to radiochemistry, Anal. Chem. 40 (1968) 586–593, https://doi.org/10.1021/ac60259a007.

[32] L. Done, M.-R. Ioan, Minimum Detectable Activity in gamma spectrometry and its use in low level activity measurements, Appl. Radiat. Isot. 114 (2016) 28–32, https://doi.org/10.1016/j.apradiso.2016.05.004.

[33] R. Gordon, Gilmore, Practical Gamma-Ray Spectrometry, second ed., John Wiley & Sons, Ltd, Chichester, 2008.

[34] T. van Dam Herman, Stefan Seifert, Winicjusz Drozdowski, Pieter Dorenbos, Dennis R. Schaart, Optical absorption length, scattering length, and refractive index of $LaBr_3$:Ce^{3+}, IEEE Trans. Nucl. Sci. 59 (2012) 656–664, https://doi.org/10.1109/TNS.2012.2193597.

[35] I.V. Khodyuk, P. Dorenbos, Nonproportional response of $LaBr_3$:Ce and $LaCl_3$:Ce scintillators to synchrotron x-ray irradiation, J. Phys. Condens. Matter 22 (2010) 485402–485408, https://doi.org/10.1088/0953-8984/22/48/485402.